Detecting mechanical property anomalies along railway earthworks by Bayesian appraisal of MASW data

A. Burzawa, L. Bodet, A. Dhemaied, M. Dangeard, Sylvain Pasquet, Q. Vitale, J. Boisson-Gaboriau, Y.J. Cui

Detecting mechanical property anomalies along railway earthworks by Bayesian appraisal of MASW data

A. Burzawa[a,b,*], L. Bodet[a], A. Dhemaied[b], M. Dangeard[b], S. Pasquet[a,c], Q. Vitale[d,e], J. Boisson-Gaboriau[b], Y. J. Cui[f]

[a] *Sorbonne Université, CNRS, EPHE, UMR 7619 METIS, 4 place Jussieu, 75252 Paris 05, France*
[b] *SNCF Réseau, 6 avenue François Mitterand 93210 Saint-Denis, France*
[c] *Observatoire des Sciences de l'Univers ECCE TERRA - UAR 3455, Sorbonne Université, CNRS, Paris, France*
[d] *Éveha International, 161 avenue de Verdun, 94200 Ivry-sur-Seine, France*
[e] *Université de Lyon, CNRS, Archeorient, UMR 5133, Maison de l'Orient et de la Méditerranée, France*
[f] *Ecole des Ponts, ParisTech*

Abstract

The techniques traditionally used to estimate the mechanical properties of railway earthworks (RE) are costly and of low performance. There is a great need for the development of non-destructive methods, which would allow a fast and efficient diagnosis of RE. Seismic surface-wave (SW) methods, also known as multi-channel analysis of surface waves (MASW), were rescaled here for there systematic implementation on RE. A test site was chosen along the North European High Speed Line (HSL) for its well-known correspondence between discontinuity in mechanical properties and anomalous maintenance forces. With the proposed acquisition and processing strategy, a contrast in SW propagation velocity was correlated with the change in shear modulus of the soil layers beneath the track, previously evaluated in

*audrey.burzawa@sorbonne-universite.fr

the laboratory. Bayesian inversion of the SW data also allowed to integrate the strong *a priori* knowledge available on these HSL lines and to provide quantitative results with a confidence index to help end-users in their decisions.

Keywords: railway earthwork, mechanical properties, seismic methods, surface waves, bayesian inversion

---

1. Introduction

The preservation and expansion of rail transportation networks is a major national and international issue. Stability problems are among the priorities. They depend mainly on the spatial and temporal variations of the mechanical properties of the materials used to build and support railway earthworks (RE). RE are dimensioned according to very strict internal construction standards (*SNCF Réseau* IN3278, IG90260 in France for instance). Unfortunately, during the life of the RE, and depending on its location and the construction period, many factors such as water drainage, weight and speed of trains, frost, etc., may cause heterogeneities in the structure of the railway tracks. It is therefore necessary to develop tools capable of monitoring the condition of the RE, to control the evolution of their mechanical state, and more particularly, improve the knowledge of existing RE assets (Selig and Waters, 1994; Trevin, 2008). Several criteria are classically used to evaluate the global track behaviour, such as geometry-related faults (cross-level, alignment, longitudinal levelling, twist and gauge) or frequency and type of maintenance operations and geotechnical surveys (Selig and Waters, 1994; Quiroga and Schnieder, 2013; Rhayma et al., 2013; Tzanakakis, 2013).

To complement the above techniques with non-destructive characterisation and imaging of the underground RE and soil structure, geophysical methods can be deployed with great efficiency and yield (Milsom and Eriksen, 2013). They are able to provide information along larger linear distances and more densely than geotechnical methods, as well as to allow interpolation of stratigraphy and mechanical parameters between boreholes. Such methods are therefore of great interest because they promise rapid and efficient diag-

nosis of the condition of RE (see for example the review on non-destructive testing methods for the assessment and monitoring of the health of railway infrastructures by Artagan et al., 2020).

In the toolbox of geophysical prospecting, it is well known that seismic methods can help, by definition, image near-surface mechanical property contrasts. This is why their use, and more particularly surface-wave (SW) based approaches, has been increasingly suggested for the investigation of RE, as for example very recently described by Kyrkou et al. (2022) in 'a review of measurement practice'. These methods, also known as Mutlichannel Analysis of Surface Waves (MASW) (see e.g. Foti et al., 2018), make it possible to estimate near-surface shear-wave velocities (V_S), hence shear moduli (G). A rationale for the use of seismic methods applied to RE and recent developments in SW techniques in this context, are presented in more details with associated references in a following section dedicated to the 'background methodology'. Despite the growing trend towards developments (Kyrkou et al., 2022), there seems to be a lack of specifically dedicated approaches best suited to the railway context.

The present study therefore aims at illustrating the feasibility of developing a specific SW prospecting method able to mechanically characterise RE and underlying soils along railway tracks, without perturbing the traffic. A test site along the North European High-Speed Line (HSL) has been targeted, as the RE at this location presented important stability problems, sufficiently documented to test new approach. To identify and understand the origin of the anomalies observed at the surface (mainly consisting in strong tracks motion and important loss of ballast), classical geotechnical

studies were conducted with core drilling, dynamic penetrometer and laboratory tests (Dhemaied et al., 2014a,b,c). We present how the geotechnical results (see more details in a dedicated section in the following) appeared non-conclusive except for laboratory measurements in soil samples of microporosimetry and V_S. These parameters, showing significant variations in one particular layer of the RE, justified the design of a specific seismic SW setup, dimensioned and adapted to this type of RE, in order to detect variations of V_S along the line. The setup and measurement strategy (array geometry, types of sensors and source) are first presented in details. To ensure reliable SW data extraction along the considered HSL, a specific processing workflow has then been suggested and detailed as well.

This work is actually presented so as to provide practitioners and end-users with detailed descriptions and guidelines of the proposed approach, seen as a toolbox to facilitate the setup design, data processing and interpretation of results. As railway infrastructure managers need thresholds above which mechanical moduli variations can be considered significant, resulting models of the RE mechanical properties are suggested here to be given in terms of probability rather than in terms of fixed parameter values with *posterior* uncertainties. This can be performed by implementing a Bayesian formalism (Tarantola, 2005). It as been applied to the appraisal of surface-wave dispersion inversion results at large scale (Sambridge, 1999b,a; Bodin et al., 2012) and, for instance, to near-surface applications with the advantage of combining different types of geophysical and geotechnical data (see e.g. Killingbeck et al., 2018; Halló et al., 2021). Following the processing workflow, the probabilistic approach implemented with the Bayesian formal-

ism as mentioned above has thus been used to enable a fair quantification of mechanical properties variations in the RE, in depth and along the line. The study finally suggests how, in the long run, such technique could be deployed with a sufficient yield for decision support, to guide choices in terms of monitoring, diagnosis and, eventually, of appropriate maintenance.

2. Background methodology

2.1. Standard track behaviour evaluation tools

Geotechnical surveys such as boreholes, coring, *in situ* testing, etc., are classically performed to test the mechanical condition of RE. Standard parameters such as the bearing capacity of base structures or the core resistance of sub-ballast layers are also regularly assessed (Benz-Navarrete, 2009; Escobar, 2015; Escobar et al., 2016; Haddani et al., 2016). But their implementation remains limited in space and extremely costly on a large scale (in France, for instance, there are more than 28,000 km of track to be monitored), not to mention the difficulties of accessing railway sites, which constitute an additional constraint and reduce the cost-effectiveness of these probing tools.

To overcome these problems, Ground Penetrating Radar (GPR) is mounted on trains and combined with high frequency levelling systems, for the imaging of RE shallow layers (detailed stratigraphy, water content and presence of mud) (see e.g. Eriksen et al., 2010; Anbazhagan et al., 2011; Hugenschmidt et al., 2013; Khakiev et al., 2014; De Bold et al., 2015). This technique however suffers limitations in depth of investigation (DOI) in high permittivity fine materials, such as clays which attenuate the signal and prevent access to underlying soils. In a similar manner, geophysical approaches of possi-

ble high yields, such as electromagnetic and capacitive electrical prospecting methods (Rejkjær et al., 2021), are very difficult to apply along railways because of their sensitivity to metallic elements, underground cables, electrical wiring systems and, of course, catenaries. Electrical Resistivity Tomography (ERT) however consists in a possible tool of interest for the study of RE, as described in details by Gunn et al. (2018). Other techniques such as microgravimetry have been suggested by geophysicists to target cavities and/or undercompacted areas (Fauchard et al., 2004; Talfumiere and Nebieridze, 2008; Nebieridze and Leroux, 2012). Yet, none of the previously mentioned methods provide information about the RE mechanical properties in the standard framework of geotechnics.

2.2. Seismic method

The mechanical parameters of shallow soil layers (compression and shear moduli) can be estimated *in situ* using seismic methods. They are based on the indirect characterization of seismic-wave propagation velocities from seismograms (records of the wavefield by means of a collection of sensors implanted at the surface and detecting the particle displacements generated by a seismic source) (see Mari et al., 2004). The refraction of body waves (compressional or pressure (P) and/or shear (S) waves), for instance, makes it possible to simply define near-surface geometry, as well as its compressional and/or shear velocities (respectively V_P and V_S). Although considered fast to implement and relatively straightforward to process, these techniques suffer from several limitations (see e.g. Mari et al., 2004; Fauchard et al., 2004). The existence of civil engineering structures with a strong 3D character and/or offering important velocity contrasts, in the vicinity of the acquisition setup

(at the surface as well as at depth), complicates the interpretation of seismograms (it becomes difficult to differentiate the various events of the wavefield which can either be due to the investigated layers at depth or to lateral '3D objects'). Conversely, refraction seismic implies the assumption of increasing velocities with depth. Lower velocity layers (LVL) will not be properly characterized and high velocity layers (HVL) will perturb the investigation of deeper structures of interest. In refraction seismic as well, accurate event detection requires a good signal-to-noise ratio (sometimes impossible to obtain in urban and suburban conditions). The study of S waves is all the more delicate, because they are more difficult to generate and identify on this type of records (Pasquet et al., 2015). It appears that the above-mentioned limitations restrict the applicability of refraction seismic (Mari et al., 2004; Fauchard et al., 2004, and moreover reflection seismic) to the characterization of RE that are typically affected by the presence of 3D structures (concrete channel for drainage and also for cables, plateforms, acces structures), HVL, LVL (high contrast between the sub-ballast layer and the capping layer), potentially significant background noise (urban context and catenary poles vibrations), etc.

From a theoretical point of view, the elastic strain generated by a mechanical dynamic source does not propagate in the Earth as body waves only. Actually, most of the energy propagates along the surface without penetrating deeply (in the upper ten meters for near-surface applications). If the mechanical properties (and more particularly the shear modulus) of the medium are vertically heterogeneous, the propagation velocity of these guided waves (the 'surface waves', also named 'PSV' or 'Rayleigh' waves in the following)

will depend on their propagation frequency. This property, called dispersion, allows us to retrieve, *via* an inversion procedure, the V_S structure of the probed medium, below the acquisition setup. Active-source SW dispersion measurements can be achieved using typical seismic shot gathers (Foti et al., 2018). The inferred V_S models are 'one-dimensional' (1D) and measurements and interpretations are limited by several well-known theoretical and experimental constraints (O'Neill, 2003; O'Neill et al., 2003; Socco and Strobbia, 2004; Bodet et al., 2005, 2009). SW methods, widely used in seismology since the 1950s, have gone through important theoretical and experimental developments for a wide range of near-surface applications since the 1980s (non-destructive evaluation, civil and geotechnical engineering, environmental geophysics, natural hazards, see Socco et al., 2010). The first applications of this technique were actually largely dedicated to the *in situ* characterization of soils and near-surface anthropogenic structures (Heisey et al., 1982; Nazarian and Stokoe II, 1984; Matthews et al., 1996; Hévin et al., 1998; Lai et al., 2002; Ryden et al., 2001, 2004). The latest methodological advances show that 'surface-wave prospecting' or MASW can be deployed along linear sections or along a surface grid, in order to reconstruct a 'two-dimensional' (2D) or 3D model of near-surface V_S distribution (Neducza, 2007; Boiero and Socco, 2010; Ezersky et al., 2013). A detailed presentation of the method, SW acquisition, processing and inversion workflows is for instance given by Pasquet and Bodet (2017), along with a tutorial for most of the codes and tools used in the following work. Further information and details can be found in the literature (see e.g. O'Neill, 2003; O'Neill et al., 2003; Socco and Strobbia, 2004; Bodet et al., 2005; Socco et al., 2010; Pasquet, 2014).

Given the guided nature of surface waves, these events of the wavefield are less sensitive to the strong 3D character of the structures encountered in civil engineering applications (Karl et al., 2011). In addition, recent studies show a growing interest in the implementation of SW prospecting related to geotechnical issues (Heitor et al., 2012) or in a railway context (Donohue et al., 2013, 2014; Hwang and Park, 2014; Forissier, 2015; Gunn et al., 2015; Bergamo et al., 2016a,b; Gunn et al., 2016; Sussmann Jr et al., 2017; Kyrkou et al., 2022), in which V_S is a very good criterion for determining the mechanical state of associated materials (see e.g. Dhemaied et al., 2014a; Byun and Tutumluer, 2017; Byun et al., 2019). However, given the specific railway environment and the geometry of the targeted structures, the experimental conditions limit the classical implementation of seismic methods (instrumental deployments are restricted both in space and time). An optimal setup configuration has thus to be defined by adapting the usual experimental protocol to the scale of RE and to the specific railway environment, while ensuring sufficient resolution for the measured velocities to be informative. Seismic methods can actually be applied to very shallow targets ($<$ 10 m depth) using various types of sources, sensor and acquisition setups, depending on the objectives (see e.g. Bachrach et al., 1998; Baker et al., 1999; Abraham et al., 2004; Schmelzbach et al., 2005), the key parameter being the measurement frequency range. Pasquet (2014); Dangeard (2019), in the same way as studies cited above, illustrated that a classical near-surface seismic sources such as a 5 kg sledgehammer (or even smaller 1.25 kg hammers available) can generate a broadband signal at frequencies high enough to reach infra-metric vertical resolutions, in media with propagation velocities lower

than 250 m.s^{-1}. In the case of RE, according to Dhemaied et al. (2014a) geotechnical results and laboratory tests, the seismic velocities can be higher than in natural unconsolidated soils (up to 600 m.s^{-1}). Care must therefore be taken to ensure that the frequencies are high enough to work at reasonable wavelengths, as for instance shown in Dangeard et al. (2021). In the following work, the strong *a priori* knowledge about RE structure along HSL and the detailed geotechnical study first presented, has made it possible to: (i) check if the setup was sufficiently simple and quick to implement (e.g. adapted to both spatial and temporal constraints along railways such as trackside occupancy limits, safety issues, operational constrains, etc.); (ii) estimate signal resolutions and anticipate for real-life data acquisitions; and (iii) verify the results provided by the inversion of SW dispersion.

3. Feasibility study along a high-speed line

3.1. Context of the test site

This study focuses on a specific location (see Figure 1) along the French north HSL (north of the town of Hattencourt) affected by an unusually frequent and local need for maintenance, more particularly observed on track 2 (V2 on Figure 1). The areas where regular and too frequent 'clogging operations' were needed (white dashed lines on Figure 1) were also strongly affected by local vertical motion of rails and sleepers at each train passage (solid white lines labelled as 'the phenomenon' on Figure 1, as observed during the geophysical survey described in the following). Since no track failures (rail, sleepers) or defects in the surface structures of the RE were observed in this area, the origins of such anomalies were assumed to be related to strong

variations in the nature or drainage of the underlying soils.

A geological and geotechnical survey has thus been suggested to better characterize the RE and underlying soils in the areas identified as problematic (Dhemaied et al., 2014a,c). The RE has been built on 'natural' loess with the typical structure defined by the *SNCF Réseau* standards (IN3278, IG90260) in terms of both geometry and mechanical properties, as shown in Figure 2 with (from top to bottom): the sub-ballast layer, the capping layer and the subgrade (mainly consisting in *in situ* soil) overlying the lithological units described bellow from core samples:

1. quaternary earthwork mainly from the RE construction and maintenance;
2. loess characterized by beige silts more or less clayey, and;
3. campanian chalk, whitish, poor in flint and possibly containing fine glaucous passages.

3.2. Standard geotechnical tests

The geotechnical study included 8 boreholes down to 3 and 12 m depths (black circles on Figure 1) as well as 5 dynamic cone penetrometer tests (DCP) 12 m deep (not presented here, see Dhemaied et al., 2014a,c; Heraibi, 2019, for more details). These *in situ* tests were complemented by laboratory measurements such as Atterberg limits, granulometry, proctor compaction tests, methylene blue values, wet bulk density and water content estimations. The results, presented by Dhemaied et al. (2014a,c), were coherent with the typical structure of HSL RE (see the Figure 2), mainly involving vertical contrasts under the ballast. These structure corresponds to: the sub-

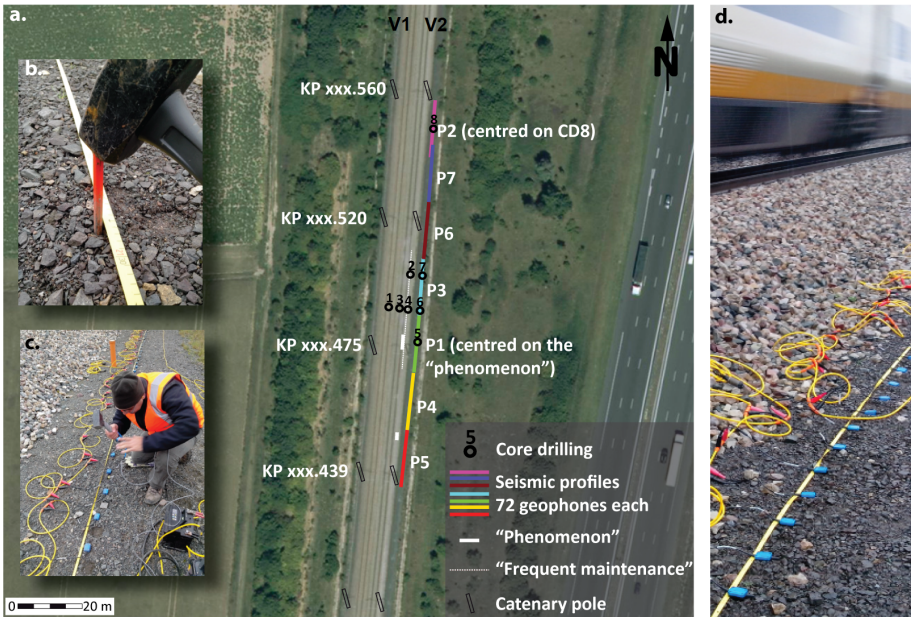

Figure 1: (a) Schematic map (modified from Bodet et al., 2017; Bodet, 2019) of the boreholes cores drillings (CD#) and seismic profiles (P1 to P7) locations. The positions of which are given according to the referenced kilometre points (KP). Local vertical motion of rails and sleepers observed at each train passage is showed by white plain lines (the phenomenon). Frequently maintained track sections are represented by the white dashed line. Photographs are given to illustrate the setups installation along the trackside: (b) preparation of the surface at each geophone location; (c) seismic source with a 1.25 kg sledgehammer vertically hitting a metallic plate; (d) setup installed along the track side.

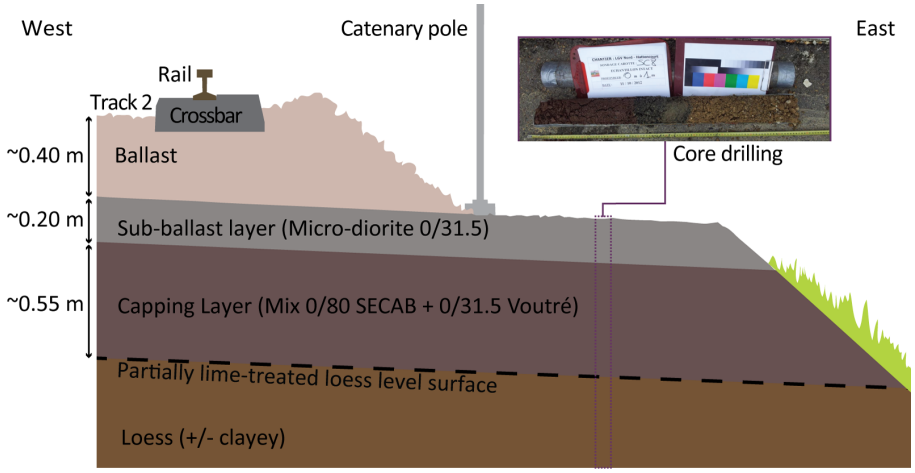

Figure 2: Schematic cross-section (modified from Bodet et al., 2017; Bodet, 2019) of the studied RE. The typical structure is defined by *SNCF Réseau* standards (IN3278, IG90260). The details about layers materials are based on 'visual' monitoring data and interpretation of core samples.

layer and the capping layer (with a total thickness of 75-80 cm on average along the track), more compact than the loess layer, itself less compact than the chalk occurring between 6 and 7 m deep under the tracks. The results also showed similar water contents and densities in the loess (respectively 20 % and between 1.6 and 1.7 Mg/m^3 between 1 and 3 m deep) whatever the locations of the drilling. The boreholes as well as the laboratory tests show neither significant variability of the RE structure along V2, nor from one trackside to another (see Dhemaied et al., 2014a,c). This type of geotechnical study therefore did not make it possible to identify the origins of the maintenance problem encountered along this line.

3.3. Shear moduli (Bender Elements) and porosimetry

To complement the classical geotechnical study summarized above, V_S measurements on samples that could be properly collected from the cores (cylindrical samples of 100 mm diameter and 50 mm height) were carried out using the 'Bender Elements' (BE) technique (Shirley and Hampton, 1978). The BE are piezoceramic plates allowing the transmission and reception of a mechanical wave through a cylindrical sample to estimate its propagation velocity (V_P or V_S according to the transmission/reception mode). This technique is widely used for the estimation of small strain shear modulus (G) in non-consolidated granular materials in general, and is the subject of active research for the study of soils in particular (see e.g. Lee and Santamarina, 2005; O'Donovan et al., 2012). The impact of water content on the propagation velocities of mechanical waves in soils was also investigated in the laboratory using this technique (Santamarina et al., 2005; Cho and Santamarina, 2001) and/or using 'acoustic' methods (see e.g. Fratta et al., 2005;

George et al., 2009). The use of BE techniques has proved interesting for the laboratory or *in situ* estimation of V_S (Byun and Tutumluer, 2017; Byun et al., 2019) in RE. G, which is an important criterion for the design and monitoring of RE's condition, can then be calculated when the density (ρ) is known as well, such as

$$G = \rho V_S^2. \quad (1)$$

For the present study, all samples were collected from the loess layer at one or several depths (depending on cores quality). The results, combined with water content and density measurements, are summarized in table 1. They show that the decrease in V_S (and consequently in G) was partly correlated with the maintenance anomaly observed along V2. Additional tests (carbonate content) showed that these results are not linked to the treatment of the loess. Finally, mercury porosimetry tests were carried out on these samples. The porosity spectra presented on Figure 3 show an increase of equivalent pore diameter, thus a variability of the microstructure, also partly consistent with the maintenance variations along V2.

3.4. Upscaling for in situ characterization of RE over long distances

Such analysis unfortunately remain sparse and time consuming, both in distance along the tracks and in depths at each sample collection location. The CD1 sample collected on V1 at 2.6 m depth (area not affected by the phenomenon, see table 1 and Figure 1), was characterised by the highest G value while its porosity spectrum was spread out. The single sample collected and analysed for CD5 showed a high G value with a marked maximum porosity while located in the problematic area. To avoid such ambiguities, regular

Table 1: Measurements of density (ρ_d), water content (w) and orders of magnitude of velocities and shear moduli ($V_{S,min-max}$ and $G_{min-max}$, respectively) measured with BE on samples collected from boreholes at on the study site. The depths correspond to the depth of the core samples centers (modified from Dhemaied et al., 2014a,b; Bodet et al., 2017; Bodet, 2019).

Core Drilling (#)	Sample depth (m)	w (%)	ρ_d (Mg/m^3)	$V_{S,min-max}$ (m.s^{-1})	$G_{min-max}$ (MPa)
CD1	1.6	20.6	1.65	120-134	28-35
CD1	2.3	15.7	1.73	125-137	30-36
CD1	2.6	15.7	1.73	596-687	675-897
CD2	2.6	19.8	1.60	165-183	52-64
CD3	1.6	18.1	1.71	152-172	44-56
CD5	1.5	20.1	1.67	312-366	185-255
CD6	1.1	20.9	1.70	153-173	44-57
CD8	2.3	19.3	1.57	296-378	166-271
CD8	2.9	15.4	1.65	357-390	242-289

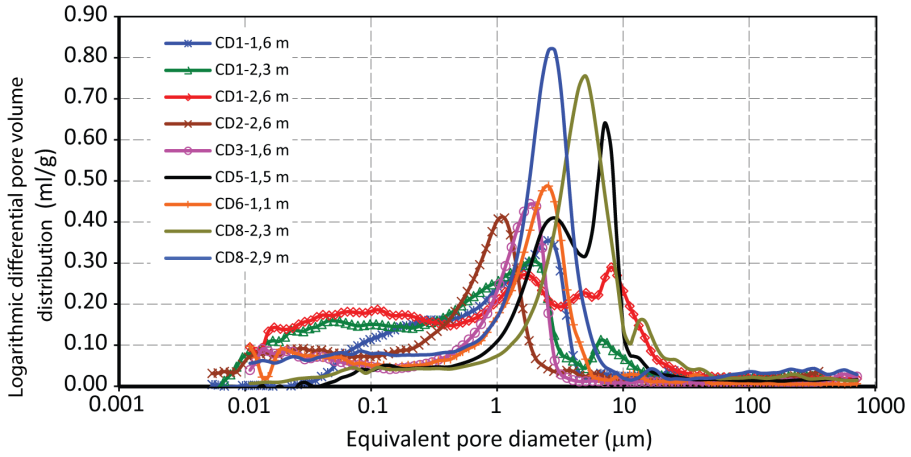

Figure 3: Mercury porosimetry measurements carried out on samples collected from boreholes (see locations on Figure 1). The depths noted in the legend correspond to the depth of the core samples centers (modified from Dhemaied et al., 2014a,b; Bodet et al., 2017; Bodet, 2019).

sampling (along the tracks as well as at depth) would be necessary. Such studies are obviously not feasible in a systematic manner for the monitoring of RE along great distances (typically tens or hundreds of kilometres). In this context, its seems justify to test seismic SW prospecting methods for a systematic non-destructive *in situ* characterisation of V_S along RE. The chosen test site is moreover extremely well constrained by HSL standards. Its recent construction (with respect to the age of conventional lines) has allows to have strong *a priori* information on the characteristics of the *in situ* soil (geometry of the RE, nature of materials, etc.) and make it convenient to perform such a feasibility study.

4. Surface-wave prospecting: implementation and dispersion measurements

4.1. Setup and measurement strategy

With dimension and acquisition parameters based both on the *a priori* well known structure of HSL RE and on properties provided by the geotechnical results presented above, 7 seismic profiles of identical length were carried out along V2 (see Figure 1a). The setup for each seismic profile consisted of 72 vertical component geophones (14 Hz low cut-off frequency) spaced with 0.25 m, so as to form a 17.75 m long profile. The setups were implanted along the trackside to ensure a good geophone coupling with near-surface materials and to avoid the particular conditions of acquisition directly on ballast (Hwang and Park, 2014; Forissier, 2015). For each seismic profile, seismic shots were performed with a 1.25 kg hammer vertically hitting a metallic plate (see Figure 1c) every 24 geophones (between adjacent geophones) with

first and last shot positions at half inter-geophone distance before and after the first and last geophone, respectively. Each shot corresponded to the stack of 6 hammer/plate impacts to improve the signal-to-noise ratio. The recording length was 2 s with a sampling interval of 0.5 ms and a pre-triggering delay of -0.02 s. The seismic profiles numbering, P1 to P7 (see Figure 1) corresponded to the implementation strategy decided during the survey:

- it was initially chosen to locate the first seismic profile at the middle of the area presenting the higher number of maintenance operations (P1 in Figure 1) and centered on CD5;
- then, another seismic profile was located at the middle of an area free of maintenance problems (P2 in Figure 1) and centered on CD8;
- 5 other seismic profiles finally made it possible to observed continuous variations between these two end-members profiles, with P5 slightly south of the high maintenance area where highly active anomalies were spotted during the survey.

The whole distance covered by these 7 seismic profiles thus represented a 120.9-m long seismic line (which is less than 7×7.75 m because of an overlap between P7 and P2 due to the original choice of centering P1 on CD5 and P2 on CD8). The acquisition parameters and the relative positions of the seismic profiles are shown in Figure 4.

The first task carried out following this survey consisted in choosing the appropriate geophone window size for the SW dispersion extraction from the recorded sets of seismograms. This method is traditionally used to ensure the best compromise between expected vertical resolution and the need to

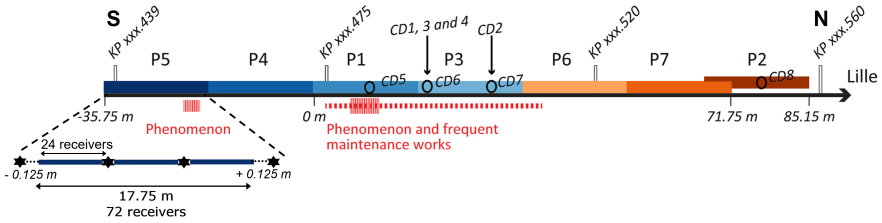

Figure 4: Schematic layout plan of the whole entire seismic line and description of a single seismic setup with 72 receivers (in blue on the left of the figure). The names of seismic profiles are written above each one. The color scale represents the position along the line with the southern seismic profiles in blue and the northern seismic profiles in orange. The position '0 m' represent the beginning of P1. The boreholes cores drilling (CD#) located above the seismic profile are represented by black circles and with black arrow when they are in the same position but offset from the track. Local vertical motion of rails and sleepers observed at each train passage (the 'phenomenon') is showed by red plain lines. Frequently maintained track sections are represented by red dashed lines.

limit the influence of lateral variations on measurements as explained in details for instance in Pasquet and Bodet (2017) (the term 'lateral variations' is sometimes used by practitioners to refer to variations encountered 'along' the seismic profile). SW dispersion analysis is indeed limited by the classical trade-off between lateral resolution and investigation depth (Gabriels et al., 1987). On the one hand, the inverse problem formulation imposes the investigated medium to be assumed 1D under the geophone spread. Additionally, the spread itself has to be short enough to achieve lateral resolution if profiling is performed. On the other hand, long geophone spreads are required in order to: obtain high resolution dispersion spectra; record wavelengths great enough to reach expected investigation depth; mitigate near-field effects; and discriminate modes at every available frequencies (see e.g. O'Neill

et al., 2003; O'Neill, 2003; Bodet et al., 2005, 2009). Several window sizes were actually processed before eventually selecting the largest one with 72 geophones, as it offered the best spectral resolution (for more details about the process, see e.g. Pasquet and Bodet, 2017; Dangeard, 2019). The choice of this window size gives a empirical maximum investigation depth (Z_{max}) of 8.875 m (based on the maximum measurable wavelength (λ_{max}), approximately equal to the length of the stacking window, divided by two, $Z \approx \lambda/2$) (Bodet et al., 2009; Pasquet and Bodet, 2017; Foti et al., 2018). In addition, as recommended by Bodet et al. (2005) and recalled by Steinel et al. (2014), direct and reverse shots on both sides of a given spread (end-on and off-end) have to be considered to check the validity of the 1D assumption according to considered wavelengths.

4.2. Seismograms

For the survey presented here, the longest spreads consisted in 72 geophones. With our acquisition setup, only 2 shots were available on both side of the spread to be systematically compared for each seismic profile. This work is illustrated here for P1 and P2 which will systematically serve as examples, since they are supposed to represent two very different states of the studied RE (the disorder zone, P1, and an area with no apparent problem, P2). Figures 5a and 5b present the 72 geophones seismograms obtained with both shots for P1 and P2, respectively. The seismic traces look symmetrical as far as the guided waves are concerned, whether it is P1 or P2. The wavefield is very clearly disturbed by the catenary pole foundations at kilometre point (KP) xxx.475 for P1 (at 5 m in local coordinates). The signal recorded along P2 is perturbed by 50 Hz noise probably because of the buried electri-

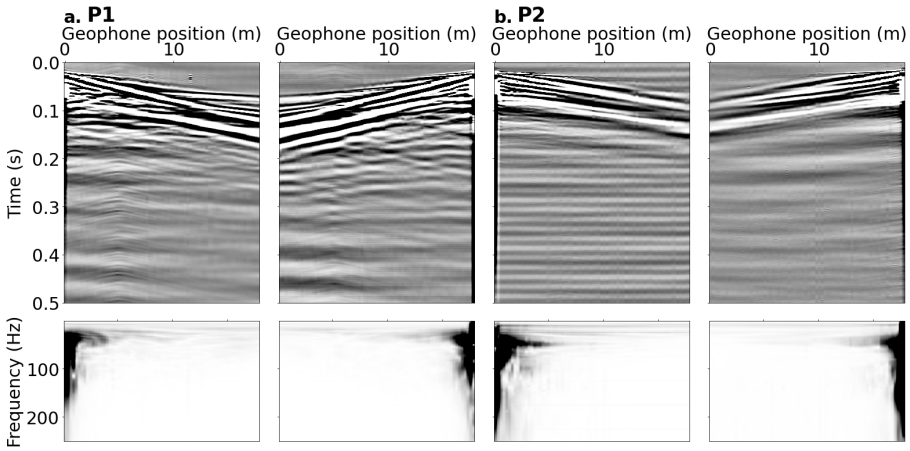

Figure 5: (a) Normalized seismograms (top) and spectrograms (bottom) of the direct and reverse shots for P1 (the geophone positions are given in the local coordinate system shown in Figure 4). The seismic traces are symmetrical with respect to the guided wave train. The spectrograms represents the frequency band along the seismic profile in which the wavefield is sufficiently energetic (maxima of amplitude in black) to allow dispersion interpretation. In (a), the wavefield is very clearly perturbed by the pole foundations at kilometre point (KP) xxx.475, around the geophone located at 5 m. In (b), the P2 shots show 50 Hz noise (probably due to the buried electrical networks and contact of the connectors with the wet ground after rain).

cal networks and a possible contact of the geophone connectors with the wet ground after rain during the survey. Strong ambient noise generated by the highway in the east produced low frequency wave fronts on both P1 and P2. As shown on spectrograms of Figures 5a and 5b, the frequency content of the data is very satisfactory as far as dispersion analysis is concerned, with significant energy from 20 Hz to at least 250 Hz.

4.3. Dispersion extraction

Each of the seismograms was then transposed, after correction for geometric attenuation, into the frequency-phase velocity domain. The result of such a wavefield transformation is called a 'dispersion image' (see the tutorial of Mokhtar et al. (1988) for more details about the slant-stack in the frequency domain). The dispersion images obtained for each shot of seismic profiles P1 and P2 are presented in Figures 6a,b and 6d,e respectively. The spectrograms are reproduced on these figures to show the frequency band in which the wavefield is sufficiently energetic to allow dispersion interpretation. Here again, whether it is P1 or P2, the direct and reverse shots produced very similar results. In this domain, the maxima (in red) on Figure 6) correspond to the dominant events of the wavefield: the PSV waves. It appears that a very large number of propagation modes are available in these images. But the difficulty of identifying their rank and the effective nature of the dispersion (Lai and Rix, 1998; O'Neill, 2003; Lin and Ashlock, 2016) only made it possible to pick the first two modes (in red and white on Figures 6c and f). The RE offers waveguides that are favourable to the emergence of higher modes, such as guided P waves, which could be interpreted in more advanced work (O'Neill et al., 2003; Maraschini et al., 2010; Boiero et al., 2013) but would involve specific processing tools not adapted to the RE context yet. The maxima of the dispersion image resulting from the summation of the two shots are also given (Figure 6c for P1 and Figure 6f for P2) and compared with the individual picks on Figure 7. It clearly shows that the obtained dispersion curves are identical (taking the errors in dispersion measurements into account, according to the relationship introduced by O'Neill (2003) and

essentially based on the resolution of the wavefield transformation).

These results validated the hypothesis of weak lateral variations along the 72 geophones window (compared to involved wavelengths). They validated the stacking of dispersion images from direct and reverse shots, for both the improvement of the signal-to-noise ratio and the mitigation of near-offset effects. Thanks to such stacking, it was also possible to preserve the highest frequency part of coherent wavefields present in the near-offset traces (O'Neill, 2003; Bodet et al., 2005, 2009). They also proved the weak influence on the dispersion analysis, of the noises identified on the seismograms as well as the repeatability of the measurement. As mentioned earlier, this work was systematically repeated for each seismic profile.

4.4. Dispersion variability along the line

As suggested by the seismograms presented previously (see Figure 5), the dispersion images and the associated picked curves obtained for P1 (Figure 6a, b and c) and P2 (Figure 6d, e and f) show a very clear difference in terms of dispersion. While the first higher mode (M1 on Figure 8) may be common to both seismic profiles for a few points, the fundamental mode (M0 on Figure 8) is clearly different from one area to another, with lower phase velocities in P1 than in P2. Since M0 is the one that reflects (very empirically) the properties of the medium, those measured in P1 and P2 suggest lower V_S in the area affected by maintenance issues. The set of dispersion data obtained for the 7 seismic profiles is finally presented on Figure 9 with a color scale according to the position along the line. Again, only M0 and M1 were safely enough identifiable in dispersion images to be picked (O'Neill and Matsuoka, 2005). The observed dispersion covers a range of wavelengths

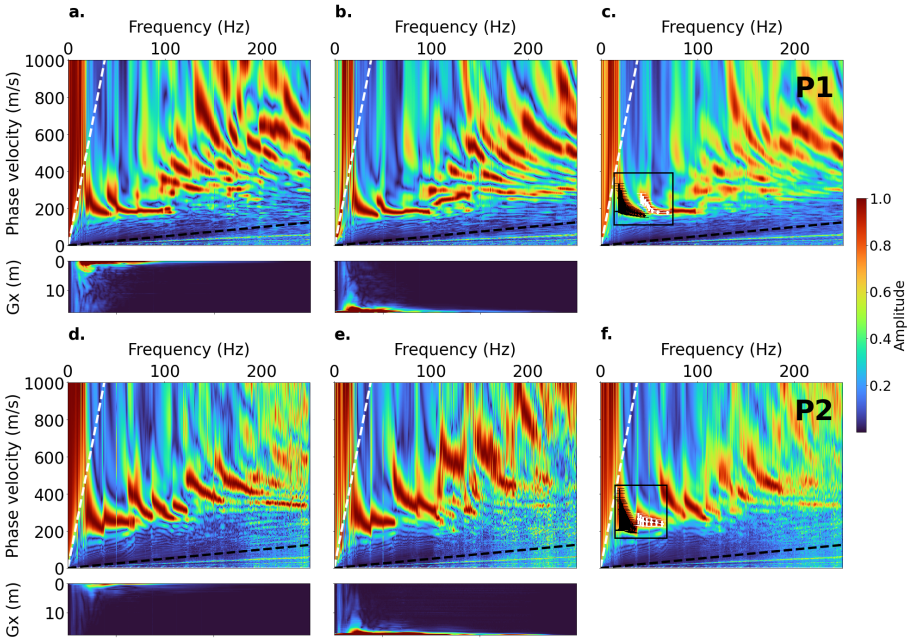

Figure 6: Normalized dispersion images and spectrograms of the direct and reverse shots (a and b for P1, d and e for P2) and stacked images for P1 (c) and P2 (f). Among the large number of propagation modes appearing on these images, only the fundamental mode (in black) and the first higher mode (in white) were picked (the errors in dispersion measurements are given empirically according to the relationship suggested by O'Neill (2003), essentially based on the resolution of the wavefield transformation). Limits of dispersion image analysis (λ_{min} and λ_{max}) are plotted in black and white dotted lines respectively. The spectrograms represent the frequency band along the seismic profile (Gx) in which the wavefield is sufficiently energetic (maxima of amplitude in red) to allow dispersion interpretation.

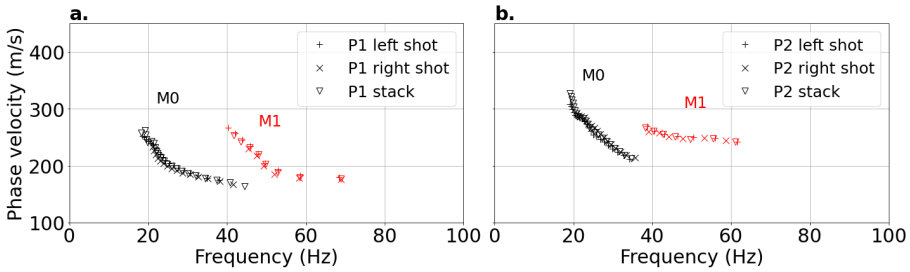

Figure 7: Dispersion data (modified from Bodet et al., 2017; Bodet, 2019) plotted for each shot at P1 (a) and P2 (b) compared to those picked from stacked dispersion images. The fundamental mode (M0) is shown in black while the first higher mode (M1) is shown in red. The data were resampled in wavelength.

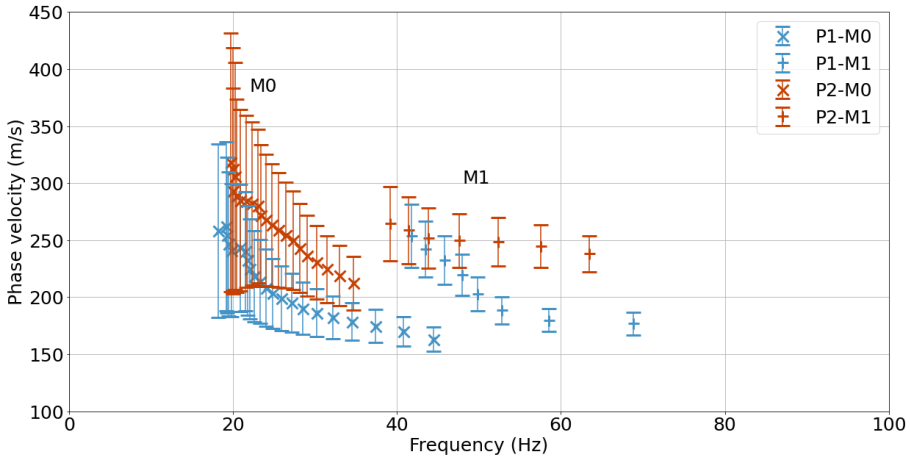

Figure 8: Comparison of the dispersion curves picked on the stacked images for P1 in blue (see Figure 6c) and P2 in orange (see Figure 6f). Only the fundamental mode (M0) and the first higher mode (M1) were considered. The data were resampled in wavelength and the error calculated according to the relation of O'Neill (2003).

(0.3 to 18 m) considered as representative of the whole RE, including the upper part of the substrate. Particular attention has been paid to the dispersion curves picking, e.g. by taking care to respect the limits related to the resolution of the wavefield transformation and near-offsets effects, as recommended by O'Neill (2003); Bodet et al. (2005, 2009) for instance. The data show a partitioning of the dispersion that clearly corresponds to the observed differences in maintenance as shown on Figure 9, with lower phase velocities in blue in the phenomenon area, and higher phase velocities in orange in the northern part of the line, with no apparent problems.

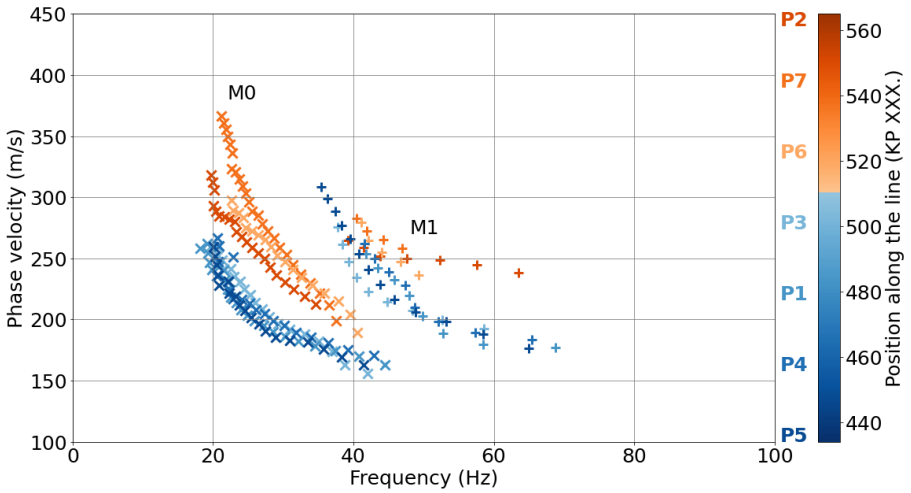

Figure 9: Dispersion curves (resampled in wavelength) plotted for every seismic profile (P1 to P7). Only the fundamental mode (M0) and the first higher mode (M1) were considered. The colorscale represents the location of seismic profiles along the line : the orange profiles are located further south (disorder area) and the blue profiles are located further north (healthy area), see Figure 4.

This is a first qualitative answer to the methodological questions posed

by the study, at least as far as this particular site is concerned. The following section will provide a more quantitative interpretation of these phase velocity measurements, by estimating 1D V_S models centered on each seismic profile, solving the classical SW dispersion inverse problem.

5. Estimating V_S along the line: the inverse problem

5.1. Extracted dispersion as data space

For each seismic profile, the data vector ($\mathbf{d}^{obs}$) to be inverted consist in N_d phase velocity measurements ($V\phi_i^{obs}$):

$$\mathbf{d}^{obs} = [V\phi_1^{obs}, V\phi_2^{obs}, \ ..., V\phi_i^{obs}, \ ..., V\phi_{N_d}^{obs}]. \quad (2)$$

When 2 modes are picked (M0 and M1), N_d is the total number of velocity measurements for M0 and M1 in their respective frequency range which can overlap or not, depending of the seismic profiles. Frequency measurements are independent variables of the problem. For each seismic profile, frequency vectors are simply sorted the same way as $\mathbf{d}^{obs}$. They thus include N_d values as well, possibly redundant when M0 and M1 are picked at the same frequencies. $V\phi_i^{obs}$ is expressed with an uncertainty σ_i simulated according to the relation of O'Neill (2003). This phase velocity uncertainty is extracted from the dispersion images and actually varies non-linearly with frequency, from the order of more than 30 % of the velocity at low frequencies to less than 1 % at high frequencies, as shown by the error bars on the selected dispersion curves for P1 and P2 on Figure 8. The uncertainties actually follow a Lorentzian distribution type at low frequencies (O'Neill, 2003), usually below 25 Hz for seismic acquisition setup used here. The implementation

of this type of uncertainty allows accounting for the poor resolution of low frequency, possible mode mis-identifications, as well as near-offset effects.

5.2. A priori information on RE and associated setup of the parameter space

HSL recently built in France (since the 1990s) are structurally well constrained (IN3278, IG90260), as presented in section 3.1 (see Figure 2). This provides very strong *a priori* information such as the number of near-surface layers, their thicknesses (H), or the approximate depth of the bedrock when geotechnical soundings are available. Based on this knowledge, the soil model of the studied RE has been built with 4 layers: the sub-ballast layer (index 1) ; the capping layer (index 2) ; a loess layer (index 3) and the half-space of chalk (index 4) (see Figure 2). The actual parameters of this soil model, as far as SW dispersion inversion is concerned, are then: H_j, V_{sj}, V_{pj} and ρ_j for each soil layer j. Finally, this represents a set of 15 parameters for this studied RE.

Ground surveys by *SNCF Réseau* confirmed the thicknesses in the study area to be in agreement with the reference thicknesses from construction standards for new HSL : 0.20 m and 0.55 m in the sub-ballast layer and the capping layer respectively (Dhemaied et al., 2014a). ρ and V_p are considered as parameters of weaker influence on SW velocity which mainly depends on the V_S structure (see e.g. the sensitivity study of Socco and Strobbia, 2004). Density values were then set according to the construction standards as well. No information was available on V_p and Poisson's ratio (ν) was set to 0.33 (which is a classical value in soils) for all layers. Table 2 summarises the fixed parameters finally chosen for this study.

The integration of all the *a priori* information on parameter values al-

Table 2: Parameters fixed according to available *a priori* information for the considered type of RE

Description of the parameter (units)	**Name**	**Value**
Thickness of the sub-ballast layer (m)	H_1	0.2
Thickness of the capping layer (m)	H_2	0.55
Poisson's ratio in every layer	ν	0.33
Density of the sub-ballast layer (kg/m^3)	ρ_1	2210
Density of the capping layer (kg/m^3)	ρ_2	2160
Density of the loess layer (kg/m^3)	ρ_3	2150
Density of the chalk layer (kg/m^3)	ρ_4	2150

lowed us to eventually constrain the model space to only 5 parameters of interest (the others being either fixed or depending on them) and thus form the following model vector $\mathbf{m}$,

$$\mathbf{m} = [V_{s1}, V_{s2}, V_{s3}, V_{s4}, H_3]. \tag{3}$$

The limits of the model space were also set according to the *a priori* information on this RE (see table 3). The borehole data (Dhemaied et al., 2014a) indicated that the thickness of the loess layer (H_3) was between 3 and 7 m. The top of the half-space depth was consequently chosen in agreement with the classical empirical relations giving the maximum investigation depth as used by practitioners and mentionned in section 4.1 ($Z_{max} \approx \lambda/2$) (see e.g. Bodet et al., 2009; Pasquet and Bodet, 2017). Preliminary inversions with greater degrees of freedom (Bodet et al., 2017; Bodet, 2019) suggested that V_{s1} and V_{s2} should not not exceed 300 m.s^{-1} and that V_{s3} should vary from 180 to 350 m.s^{-1}, depending on the considered zone (as confirmed by

Table 3: Parameter space, boundaries and sampling interval: shear-wave velocity of the sub-ballast layer (V_{S1}), shear-wave velocity of the capping layer (V_{S2}), shear-wave velocity of the loess (V_{S3}), shear-wave velocity of the chalk (V_{S4}) and thickness of the loess (H_3). This parameterisation creates a space composed of $N_m = 907,200$ possible models.

Parameter name (unit)	**Min value**	**Max value**	**Sampling interval**	**Number of possible values**
V_{S1} ($m.s^{-1}$)	50	270	11	21
V_{S2} ($m.s^{-1}$)	60	130	7	10
V_{S3} ($m.s^{-1}$)	180	350	10	18
V_{S4} ($m.s^{-1}$)	300	600	20	15
H_3 (m)	3	7	0.25	16

BE data). V_{S4} was authorized to vary in a range of 300 $m.s^{-1}$ to 600 $m.s^{-1}$, as suggested by maximum apparent velocities observed in the data. The velocity sampling step (see table 3) was defined according to the dispersion resolution and uncertainty: with greater steps for deeper layers empirically corresponding to the dispersion response at low frequencies and ; with smaller steps for shallow layers empirically corresponding to the dispersion response at high frequencies. According to empirical relationships used by the community as well (see e.g. O'Neill, 2003; Bodet et al., 2005; Dangeard et al., 2018), the best possible resolution in thickness was estimated equal to the seismograms space sampling interval (25 cm). This parameterisation finally leads to a space of $N_m = 907,200$ possible models.

5.3. Retrieving V_S from dispersion data in a Bayesian framework

From the parameter space described above, a basic grid search algorithm is used to build the following misfit function:

$$misfit(\mathbf{m}) = \sum_{i=1}^{N_d} \frac{(\mathrm{V}\phi_i^{calc} - \mathrm{V}\phi_i^{obs})^2}{\sigma_i^2}, \tag{4}$$

where $\mathrm{V}\phi_i^{calc}$ are the elements, at each measurements frequency, of the synthetic data vector ($\mathbf{d}^{calc}$) computed for $\mathbf{m}$ using the Thomson-Haskell matrix propagator method (Thomson, 1950; Haskell, 1953), as classically used to provide theoretical SW dispersion curves in horizontally stratified media. An example of the results provided by the grid search is given in Figure 10. It shows all dispersion curves and associated $\mathrm{V_S}$ models represented according to their corresponding *misfit* value, for the data collected along P1 (Figure 10a, b) and P2 (Figure 10c, d). In theory, the solution of the inverse problem (if it exists) is the minimum of the *misfit* function.

Misfit minima for the parameter $\mathrm{V_{S1}}$ are observed around 80 m.s^{-1} for P1 and 210 m.s^{-1} for P2. In contrast, $\mathrm{V_{S2}}$ for P1 shows minimum misfit values around 100 m.s^{-1} while for P2 the minima are around 75 m.s^{-1}. As expected from BE data, the minima of the misfit show higher $\mathrm{V_{S3}}$ for P2 than for P1, with velocity of the order of 300 m.s^{-1} and 210 m.s^{-1} respectively. The parameters $\mathrm{H_3}$ and $\mathrm{V_{S4}}$ do not present distinct misfit minima for their part, which means that it is not possible to find unique valuable values for these parameters and that the chalk layer might be deeper than the maximum investigation depth.

In order to present these grid search results with an estimation of their reliability, they have been expressed, as suggested by Tarantola and Valette

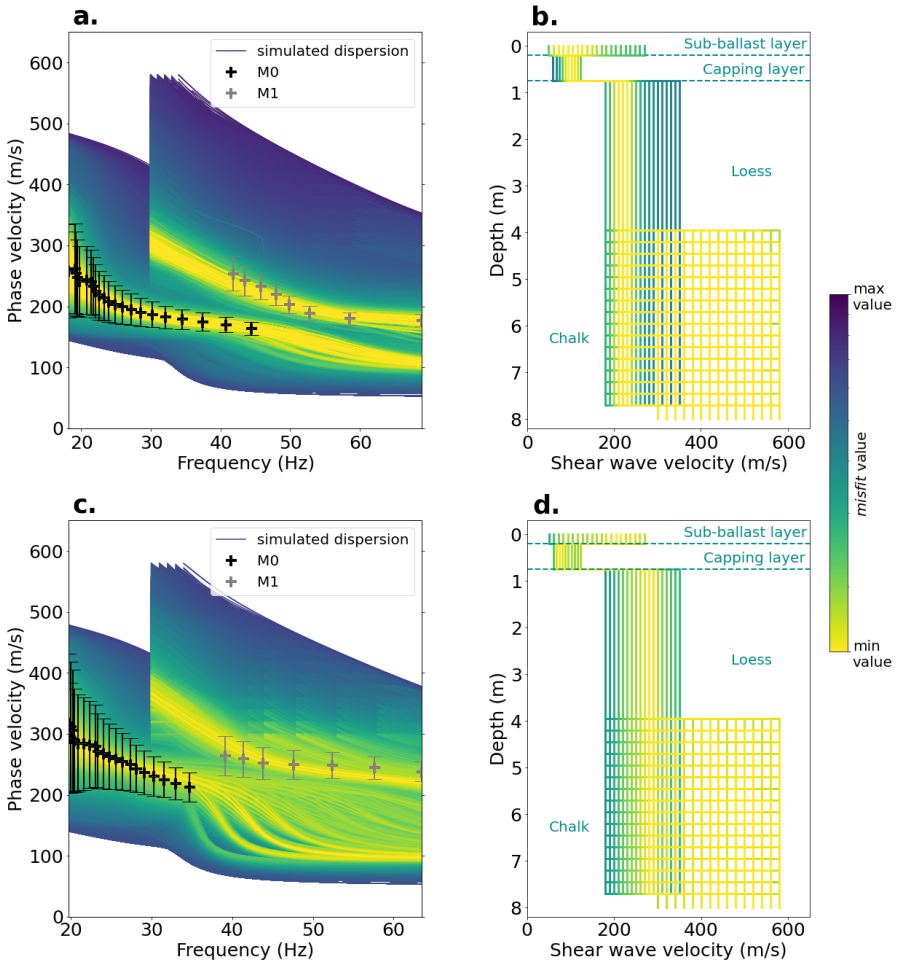

Figure 10: Grid search results: at the top for P1 (a, b) and at the bottom for P2 (c, d). (a) and (c) show dispersion curves with the fundamental mode (M0) and the first higher mode (M1). (b) and (d) represent velocity models. Each dispersion curve and each velocity model are shown with a color depending on the misfit value between the data (black dots and error bars) and the simulated dispersion. The data were resampled in wavelength and the error has been calculated according to the relation of O'Neill (2003).

(1982); Tarantola (2005), in terms of the *a posteriori* probability density function (*pdf*) $\sigma(\mathbf{m}|\mathbf{d}^{obs})$, through the application of the Bayes' theorem:

$$\sigma(\mathbf{m}|\mathbf{d}^{obs}) = \frac{p(\mathbf{d}^{obs}|\mathbf{m})\rho(\mathbf{m})}{\int_{\mathcal{M}} p(\mathbf{d}^{obs}|\mathbf{m})\rho(\mathbf{m})d\mathbf{m}}, \tag{5}$$

where $\sigma(\mathbf{m}|\mathbf{d}^{obs})$ estimates the probability to recover the 1D V_S vertical structure of the RE below each seismic profile along the line, knowing the phase velocity data and associated uncertainties. $\rho(\mathbf{m})$ is the *a priori pdf* which contains all the information available on the RE structure and properties of the subsurface even before acquiring the phase velocity data. The actual *a priori* are the limits (minimum and maximum possible values) of the parameter space $\mathcal{M}$, as described earlier in Table 3. It thus consists in the uniform *a priori* and has been defined homogeneous throughout the model space with

$$\rho(\mathbf{m}) = 1/N_m \ . \tag{6}$$

$p(\mathbf{d}^{obs}|\mathbf{m})$, on its side, is the function which sets the likelihood of every 1D V_S vertical models of the RE as defined in the parameter space, when the phase velocity dispersion that could be calculated from them ($\mathbf{d}^{calc}$) is compared to actually measured data ($\mathbf{d}^{obs}$). As mentioned above, the comparison was performed (in the grid search) considering that measured phase velocity data have uncertainties and that the visited models do not reproduce them perfectly, so the likelihood depends on the misfit function in the following manner:

$$p(\mathbf{d}^{obs}|\mathbf{m}) = e^{-\frac{1}{2}misfit(\mathbf{m})} \ . \tag{7}$$

The *a posteriori pdf* $\sigma(\mathbf{m}|\mathbf{d}^{obs})$ are given as example for P1 and P2 on Figure 11 and Figure 12, respectively. These figures show, in a matrix format

for every parameters at once, every possible 2D marginal *pdfs* in order to reveal possible covariances, as well as the 1D *a priori* and *a posteriori* marginal *pdf*s (on the diagonal of Figure 11 and Figure 12). For both P1 and P2, the 2D marginal *pdfs* show very clearly that the systematic grid search does not suggest any distinct solution for H_3 nor for V_{S4}. The velocities of the 3 first layers seem on the other hand well defined in the *a priori* limits. The 2D marginal *pdfs* indeed show Gaussian shapes with unique maxima, in particular quite distinct for the (V_{S2}, V_{S3}) couple. These two parameters appear to be very different depending on the measurement position along the line.

These *a posteriori pdf* $\sigma(\mathbf{m}|\mathbf{d}^{obs})$ have been computed for every seismic profiles and the marginal *a posteriori pdf* associated to each parameters are presented in Figure 13. As clearly shown on the 2D marginals, the parameters V_{S4} and H_3 are not well defined (1D marginals *pdf*s do not present Gaussian shapes neither clearly identifiable maxima). The *a posteriori* marginal *pdf*s of V_{S1} do not seem to be well defined, as they does not show neither clear Gaussian shapes or unique maxima, except for P3. It is therefore difficult to interpret the behaviour of the mechanical state in the sub-ballast layer along the study zone. The marginal *a posteriori pdfs* for V_{S2} are not very well defined neither. Yet, the *pdfs* suggest slightly higher V_{S2} on the southern part of the line compared to the northern part. In contrast, for V_{S3}, *pdfs* clearly show two distinct groups with lower velocities in the disorder zone compared to the 'healthy' area. The most important feature here is that these *pdfs*, which do not overlap in velocity (their width are different due to the contrast of velocity, hence corresponding uncertainty), do show a partitioning in very good agreement with BE data and analyses presented earlier.

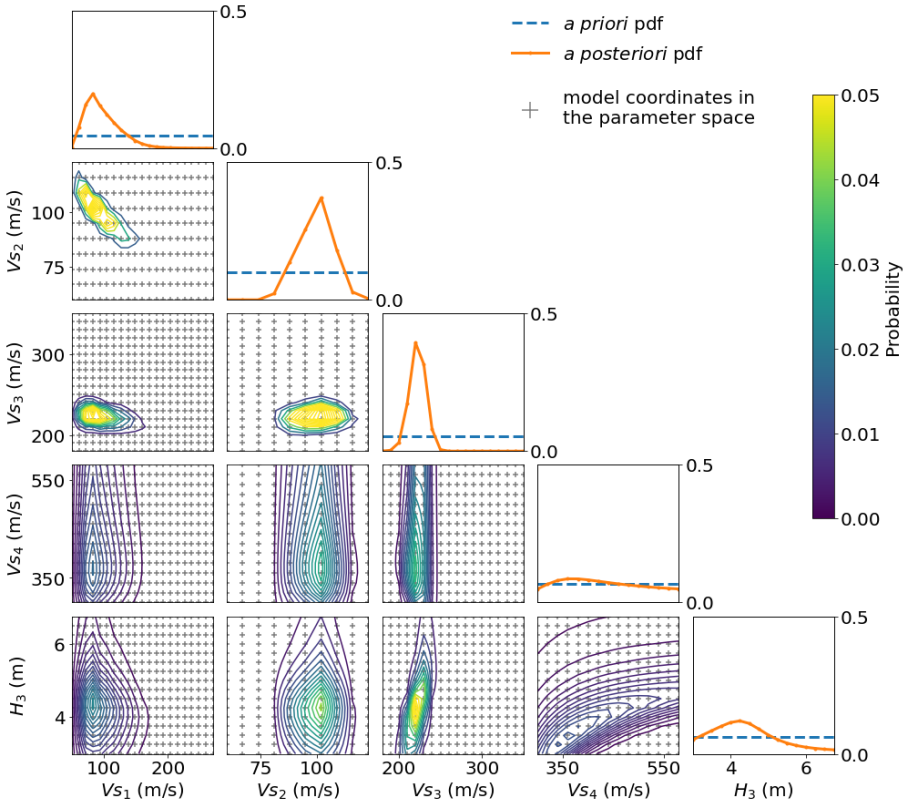

Figure 11: Bayesian appraisal of the grid search for P1, presented as a cornerplot. The diagonal presents the *a posteriori pdf* (in orange) for each parameter (label and legend given along the x-axis, the y-axis giving the probability value). The homogeneous *a priori pdf* is given in blue dashed lines. The other plots represent the *a posteriori* marginal *pdf* per pair of parameters (labels and legend presented along the x and y-axis). The colorbar present the probability value. The grey plus sign indicates the model coordinates in the parameter space.

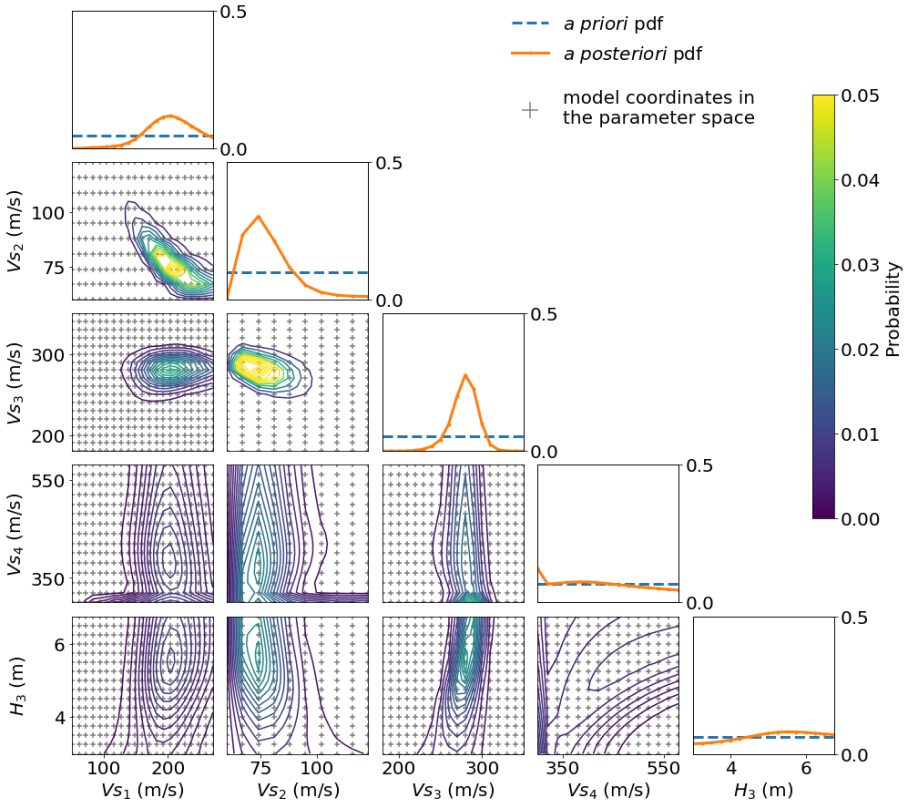

Figure 12: Bayesian appraisal of the grid search for P2, presented as a cornerplot. The diagonal presents the *a posteriori pdf* (in orange) for each parameter (label and legend given along the x-axis, the y-axis giving the probability value). The homogeneous *a priori pdf* is given in blue dashed lines. The other plots represent the *a posteriori* marginal *pdf* per pair of parameters (labels and legend presented along the x and y-axis). The colorbar present the probability value. The grey plus sign indicates the model coordinates in the parameter space.

As shown above, the parameter that shows the best definition of *pdf* maxima and strong partitioning is V_{S3}.

To go further, the marginal *a posteriori pdf* on G in the loess layer (G_3) was inferred in a Bayesian framework as well and presented in Figure 14. These results show the same behaviour, i.e. G_3 in the northern profiles is clearly higher than in the southern profiles. The results can be compared with the laboratory tests presented in section 3.3, yet only qualitatively since these moduli are inferred from soil samples with average values per layer and under different state of stress. The comparable samples are from CD2 and CD8 (see Table 1) at 2.6 m and 2.9 m and located on P3 and P2, respectively. CD2 is representative of the medium at the southern part of the profile with low G values (of 52-64 MPa) while CD8 is typical of the good RE state with higher values (around 242-289 MPa).

6. Conclusions

Samples previously collected and studied in the RE along the targeted site, originally showed that laboratory V_S measurements and microporosity were the only data able to identify the origin of maintenance anomalies, when classical geotechnical approaches (*in situ* or laboratory tests) would fail. V_S thus appeared as a good indicator of the mechanical quality of materials in the RE. These results made it possible to propose this area of the France northern HSL as a test site for the development of non-destructive and more efficient methods to monitor RE. SW techniques with small size setups were thus suggested to estimate V_S along these structures (HSL RE). SW acquisitions proved their advantage of robustness against noise and influence of

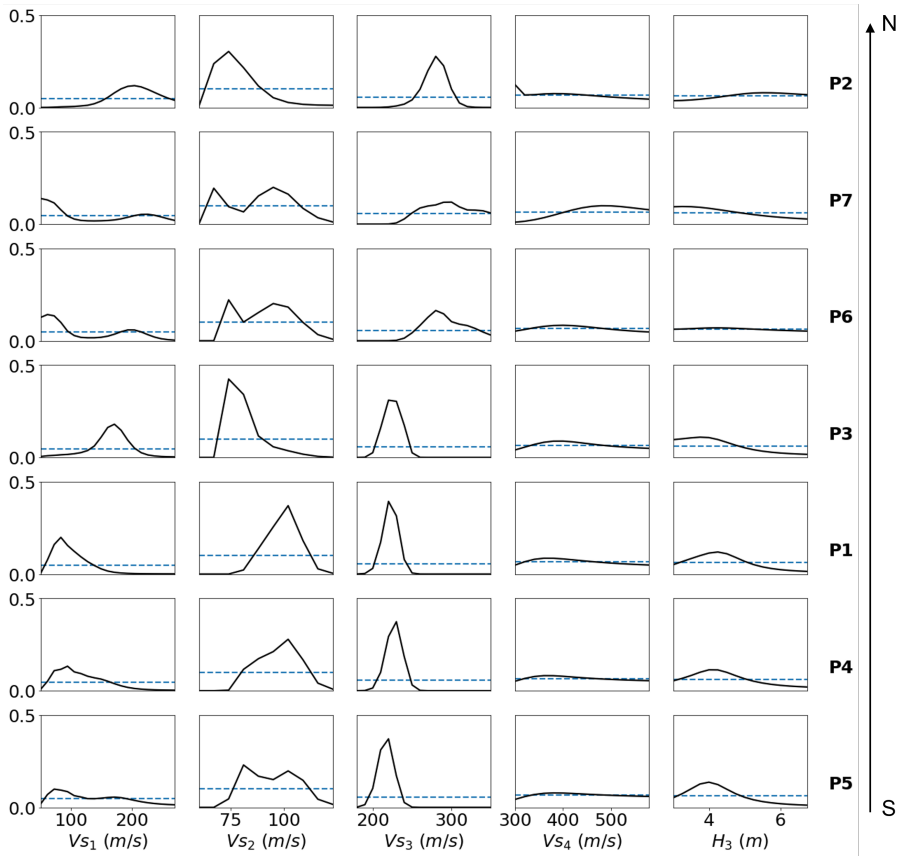

Figure 13: Marginal *pdf*s of each parameters of the Bayesian inversions performed for each seismic profiles. The profiles are ordered according to their position along the line (see figure 4). The blue dotted lines represent the *a priori* mariginal *pdf*s and the black lines represent the *a posteriori* marginal *pdf*s.

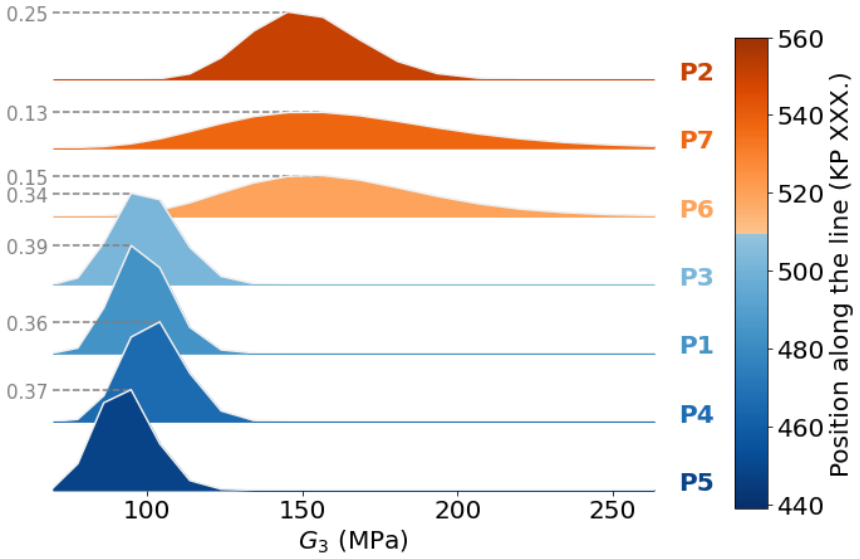

Figure 14: Synthetic representation of the Bayesian inversions performed along the line for the *a posteriori* marginal *pdf* of G_3. The seismic profiles are ordered and colored according to their position along the line: the orange profiles are located further south (disorder area) and the blue profiles are located further north (healthy area), see Figure 4. The grey values on the left are the probabilities of each maxima (the *pdf s* are ploted with equal vertical scales).

3D structures in this particular context. The systematic record of both direct and reverse shots seismograms allowed reliable and repeatable dispersion measurements along the trackside. This approach, combined with dispersion image stacking, offered sufficient spectral resolution in wide frequency and velocity ranges. The dispersion images have then been meticulously analysed and the choice of picking only the fundamental and first higher mode was made. This was assumed to be the best compromise between the amount of information accessible in the dispersion image and the safe identification and inversion of propagation modes. 7 seismic profiles, intercepting the area of unusual maintenance works, then produced very distinct SW propagation velocities (correlated with the previously identified phenomenon). The strong *a priori* knowledge available for this type of RE structure, allowed a very well constrained inversion of dispersion data for 1D models of V_S along the trackside. The inversion of each profile has been proposed in a Bayesian framework, in order to estimate the *a posteriori pdf* on V_S for each layer of the RE. The presentation of these *a posteriori pdf* for every profiles clearly showed a partitioning, particularly marked in the loess layer, that corresponds to the observed RE stability issues. Thanks to the Bayesian framework chosen for dispersion data interpretations, the suggested method enabled the estimation of shear moduli in the affected layer, with levels of confidence. These results are very encouraging with regards to the applicability of the developed approach in an industrial manner, with the possibility to consider it as a decision support tool. However, the methodology presented in this article, remains to be validated in different contexts, and above all to be optimised for large scale deployments. Several aspects have to thus be

addressed, such as the development of an operational and versatile methodology (e.g. adaptable to the variety of RE 'heritage' and the diversity of *pathologies* to be diagnosed). In order to achieve this, it will be necessary to fully extract all the available information from the dispersion images. It is therefore planned to develop tools for more automatic dispersion analysis and inversion (using machine and/or deep learning algorithms). The systematic implementation of the method eventually requires the design of deployment tools with sufficiently high yield to support decision-making and to guide choices in terms of monitoring and maintenance.

Acknowledgements

This work has been funded by *SNCF Réseau/CNRS/Université Pierre et Marie Curie-Paris6/Sorbonne Université* research contracts C13/411, C15/0781 and the convention *ANRT/Cifre-SNCF Réseau* C21/1995. The geophysical equipment was provided by the METIS laboratory at *Sorbonne Université*. The authors thank SNCF Réseau local teams for there great help and support during field works. Seismic data processing has been performed thanks to open-source software packages: SWIP (github.com/SWIPdev/SWIP/releases), Seismic Unix (github.com/JohnWStockwellJr/SeisUnix) and GEOPSY (geopsy.org). The authors thank A-M. Tang, J.-M. Terpereau, P. Leroux, A. Robinet and S. Nebieridze for their advices and support during the study, as well as valuable discussion for the results interpretations.

References

Abraham, O., Chammas, R., Cote, P., Pedersen, H.A., Semblat, J.F., 2004. Mechanical characterization of heterogeneous soils with surface waves: experimental validation on reduced-scale physical models. Near Surface Geophysics 2, 249–258. doi:https://doi.org/10.3997/1873-0604.2004022.

Anbazhagan, P., Lijun, S., Buddhima, I., Cholachat, R., 2011. Model track studies on fouled ballast using ground penetrating radar and multichannel analysis of surface wave. Journal of Applied Geophysics 74, 175–184. doi:https://doi.org/10.1016/j.jappgeo.2011.05.002.

Artagan, S.S., Ciampoli, L.B., D'Amico, F., Calvi, A., Tosti, T., 2020. Non-destructive assessment and health monitoring of railway infrastructures. Surveys in Geophysics 41, 447–483. URL: https://link.springer.com/article/10.1007/s10712-019-09544-w.

Bachrach, R., Dvorkin, J., Nur, A., 1998. High-resolution shallow-seismic experiments in sand, part ii: Velocities in shallow unconsolidated sand. Geophysics 63, 1234–1240. doi:https://doi.org/10.1190/1.1444424.

Baker, G.S., Steeples, D.W., Schmeissner, C., 1999. In-situ, high-frequency p-wave velocity measurements within 1 m of the earth's surface. Geophysics 64, 323–325. doi:https://doi.org/10.1190/1.1444537.

Benz-Navarrete, M.A., 2009. Mesures Dynamiques lors du battage du pénétromètre PANDA 2. Ph.D. thesis. Universite Blaise Pascal - Clermont II. France. URL: https://www.theses.fr/2009CLF21930, doi:tel-00725564.

Bergamo, P., Dashwood, B., Uhlemann, S., Swift, R., Chambers, J., Gunn, D., Donohue, S., 2016a. Time-lapse monitoring of climate effects on earthworks using surface waves. Geophysics 81, EN1–EN15. doi:https://doi.org/10.1190/geo2015-0275.1.

Bergamo, P., Dashwood, B., Uhlemann, S., Swift, R., Chambers, J.E., Gunn, D.A., Donohue, S., 2016b. Time-lapse monitoring of fluid-induced geophysical property variations within an unstable earthwork using P-wave refraction. Geophysics 81, EN17–EN27. doi:https://doi.org/10.1190/geo2015-0276.1.

Bodet, L., 2019. Surface waves modelling and analysis in media of increasing degrees of complexity. Thesis manuscript preprint for the "Habilitation à diriger des recherches". Sorbonne Université. France. URL: https://hal.sorbonne-universite.fr/tel-02866882.

Bodet, L., Abraham, O., Clorennec, D., 2009. Near-offsets effects on rayleigh-wave dispersion measurements: Physical modelling. Journal of Applied Geophysics 68, 95–103. doi:https://doi.org/10.1016/j.jappgeo.2009.02.012.

Bodet, L., Rahmania, I., Kyrkou, K., Wacquier, L., Dangeard, M., Pasquet, S., Vitale, Q., Dhemaied, A., Boisson-Gaboriau, J., Nebieridze, S., 2017. Estimation in situ des variations de propriétés mécaniques de la plateforme ferroviaire par ondes sismiques de surface. Internal report, in French. SNCF.

Bodet, L., van Wijk, K., Bitri, A., Abraham, O., Côte, P., Grandjean, G.,

Leparoux, D., 2005. Surface-wave inversion and limitations from laser-doppler and physical modeling. Journal of Environmental and Engineering Geophysics 10, 151–162. doi:https://doi.org/10.2113/JEEG10.2.151.

Bodin, T., Sambridge, M., Tkalčić, H., Arroucau, P., Gallagher, K., Rawlinson, N., 2012. Transdimensional inversion of receiver functions and surface and wave dispersion. Journal of Geophysical Research 117. doi:10.1029/2011JB008560.

Boiero, D., Socco, L.V., 2010. Retrieving lateral variations from surface wave dispersion curves. Geophysical Prospecting 58, 977–996. doi:10.1111/j.1365-2478.2010.00877.x.

Boiero, D., Wiarda, E., Vermeer, P., 2013. Surface- and guided-wave inversion for near-surface modeling in land and shallow marine seismic data. The Leading Edge 32, 638–646. doi:https://doi.org/10.1190/tle32060638.1.

Byun, Y.H., Tutumluer, E., 2017. Bender elements successfully quantified stiffness enhancement provided by geogrid–aggregate interlock. Transportation Research Record 2656, 31–39. doi:https://doi.org/10.3141/2656-04.

Byun, Y.H., Tutumluer, E., Feng, B., Kim, J.H., Wayne, M.H., 2019. Horizontal stiffness evaluation of geogrid-stabilized aggregate using shear wave transducers. Geotextiles and Geomembranes 47, 177–186. doi:https://doi.org/10.1016/j.geotexmem.2018.12.015.

Cho, G., Santamarina, J., 2001. Unsaturated particulate materials—particle-level studies. Journal of Geotechnical and Geoenvironmental Engineering 127, 84–96. doi:https://doi.org/10.1061/(ASCE)1090-0241(2001)127:1(84).

Dangeard, M., 2019. Développement d'une approche " time-lapse " des méthodes sismiques pour l'hydrogéophysique et la compréhension de la dynamique des hydrosystèmes. Theses. Sorbonne Université. France. URL: https://tel.archives-ouvertes.fr/tel-02931838.

Dangeard, M., Bodet, L., Pasquet, S., Thiesson, J., Guérin, R., Jougnot, D., Longuevergne, L., 2018. Estimating picking errors in near-surface seismic data to enable their and time-lapse interpretation of hydrosystems. Near Surface Geophysics 16, 613–625. doi:https://doi.org/10.1002/nsg.12019.

Dangeard, M., Rivière, A., Bodet, L., Schneider, S., Guérin, R., Jougnot, D., Maineult, A., 2021. River corridor model constrained by time-lapse seismic acquisition. Water Resources Research 57. doi:https://doi.org/10.1029/2020WR028911.

De Bold, R., O'Connor, G., Morrissey, J., Forde, M., 2015. Benchmarking large scale GPR experiments on railway ballast. Construction and Building Materials 92, 31–42. doi:https://doi.org/10.1016/j.conbuildmat.2014.09.036.

Dhemaied, A., Cui, Y.J., M., T.A., 2014a. Etude de la sensibilité de la

raideur mécanique des sols supports à la variation de la teneur en eau. Rapport d'activité. ENPC/SNCF.

Dhemaied, A., Cui, Y.J., Tang, A.M., Nebieridze, S., Terpereau, J.M., Leroux, P., 2014b. Effet de l'état hydrique sur la raideur mécanique, in: GEORAIL 2014.

Dhemaied, A., Cui, Y.J., Tang, A.M., Nebieridze, S., Terpereau, J.M., Leroux, P., Bodet, L., Pasquet, S., 2014c. Caractérisation des sols prélevés in situ, in: GEORAIL 2014.

Donohue, S., Forristal, D., Donohue, L.A., 2013. Detection of soil compaction using seismic surface waves. Soil and Tillage Research 128, 54–60. doi:https://doi.org/10.1016/j.still.2012.11.001.

Donohue, S., Gunn, D.A., Bergamo, P., Hughes, E., Dashwood, B., Uhlemann, S., Chambers, J.E., Ward, D., 2014. Assessing climate effects on railway earthworks using MASW, in: Near Surface Geoscience 2014 - 20th European Meeting of Environmental and Engineering Geophysics, pp. 1–5. doi:https://doi.org/10.3997/2214-4609.20141995.

Eriksen, A., Gascoyne, J., Mangan, C., Fraser, R., 2010. Practical applications of gpr surveys for trackbed characterisation in the uk, ireland, usa and australia, in: CORE 2010: Rail, Rejuvenation and Renaissance. URL: https://zeticarail.com/wp-content/uploads/2017/02/Applications-of-GPR-Surveys-for-Trackbed-Characterisation.pdf.

Escobar, E., Navarrete, M.B., Gourvès, R., Haddani, Y., Breul, P., Chevalier, B., 2016. Dynamic Characterization of the Supporting Layers in Railway Tracks using the Dynamic Penetrometer Panda 3®. Procedia Engineering 143, 1024–1033. doi:https://doi.org/10.1016/j.proeng.2016.06.099.

Escobar, E.J.V., 2015. Mise au point et exploitation d'une nouvelle technique pour la reconnaisance des sols : le PANDA 3. Ph.D. thesis. Université Blaise Pascal - Clermont-Ferrand II. France. URL: https://www.theses.fr/2015CLF22570.

Ezersky, M.G., Bodet, L., Akawwi, E., Al-Zoubi, A.S., Camerlynck, C., Dhemaied, A., Galibert, P.Y., 2013. Seismic surface-wave prospecting methods for sinkhole hazard assessment along the dead sea shoreline. Journal of Environmental and Engineering Geophysics 18, 233–252. doi:https://doi.org/10.2113/JEEG18.4.233.

Fauchard, C., Pothérat, P., Cote, P., Mudet, M., 2004. Détection de cavités souterraines par méthodes géophysiques. Laboratoire Central des Ponts et Chaussées.

Forissier, D., 2015. Caractérisation de la compacité du ballast ferroviaire par méthodes sismiques. Ph.D. thesis. École doctorale Sciences, Ingénierie et Environnement, Université Paris-Est. France. URL: https://www.theses.fr/2015PESC1184.

Foti, S., Hollender, F., Garofalo, F., Albarello, D., Asten, M., Bard, P.Y., Comina, C., Cornou, C., Cox, B., Di Giulio, G., Forbriger, T., Hayashi, K., Lunedei, E., Martin, A., Mercerat, D., Ohrnberger, M., Poggi, V.,

Renalier, F., Sicilia, D., Socco, V., 2018. Guidelines for the good practice of surface wave analysis: a product of the interPACIFIC project. Bulletin of Earthquake Engineering 16, 2367–2420. doi:https://doi.org/10.1007/s10518-017-0206-7.

Fratta, D., Alshibli, K., Tanner, W., Roussel, L., 2005. Combined tdr and p-wave velocity measurements for the determination of in situ soil density—experimental study. Geotechnical Testing Journal 28. doi:10.1520/GTJ12293.

Gabriels, P., Snieder, R., Nolet, G., 1987. In situ measurements of shear-wave velocity in sediments with higher-mode Rayleigh waves. Geophysical Prospecting 35, 187–196. doi:https://doi.org/10.1111/j.1365-2478.1987.tb00812.x.

George, L.A., Dewoolkar, M.M., Znidarcic, D., 2009. Simultaneous laboratory measurement of acoustic and hydraulic properties of unsaturated soils. Vadose Zone Journal 8, 633–642. doi:https://doi.org/10.2136/vzj2008.0139.

Gunn, D., Chambers, J., Dashwood, B., Lacinska, A., Dijkstra, T., Uhlemann, S., Swift, R., Kirkham, M., Milodowski, A., Wragg, J., Donohue, S., 2018. Deterioration model and condition monitoring of aged railway embankment using non-invasive geophysics. Construction and Building Materials 170, 668–678. doi:https://doi.org/10.1016/j.conbuildmat.2018.03.066.

Gunn, D., Chambers, J., Uhlemann, S., Wilkinson, P., Meldrum, P., Di-

jkstra, T., Haslam, E., Kirkham, M., Wragg, J., Holyoake, S., Hughes, P., Hen-Jones, R., Glendinning, S., 2015. Moisture monitoring in clay embankments using electrical resistivity tomography. Construction and Building Materials 92, 82–94. doi:https://doi.org/10.1016/j.conbuildmat.2014.06.007.

Gunn, D., Dashwood, B.A., Bergamo, P., Donohue, S., 2016. Aged embankment imaging and assessment using surface waves. Proceedings of the Institution of Civil Engineers-Forensic Engineering 169, 149–165. doi:https://doi.org/10.1680/jfoen.16.00022.

Haddani, Y., Breul, P., Saussine, G., Navarrete, M.A.B., Ranvier, F., Gourvès, R., 2016. Trackbed mechanical and physical characterization using PANDA®/geoendoscopy coupling. Procedia Engineering 143. doi:https://doi.org/10.1016/j.proeng.2016.06.118.

Halló, M., Imperatori, W., Panzera, F., Fäh, D., 2021. Joint multizonal transdimensional bayesian inversion of surface wave dispersion and ellipticity curves for local near-surface imaging. Geophysical Journal International 226, 627–659. doi:https://doi.org/10.1093/gji/ggab116.

Haskell, N.A., 1953. The dispersion of surface waves on multilayered media. Bulletin of the seismological society of America 43, 17–346. doi:https://doi.org/10.1785/BSSA0430010017.

Heisey, J., Stokoe II, K., A.H, M., 1982. Moduli of Pavement and Systems from Spectral and Analysis of Surface and Waves. Transportation Research

Record 852, 22–31. URL: https://onlinepubs.trb.org/Onlinepubs/trr/1982/852/852-004.pdf.

Heitor, A., Indraratna, B., Rujikiatkamjorn, C., Golaszewski, R., 2012. Characterising compacted fills at penrith lakes development site using shear wave velocity and matric suction, in: 11th Australia - New Zealand Conference on Geomechanics: Ground Engineering in a Changing World, Melbourne, Australia. pp. 1262–1267. URL: https://ro.uow.edu.au/engpapers/4431/.

Heraibi, R., 2019. Optimisation du profilage par ondes de surface pour la reconnaissance des plateformes ferroviaires. Master's thesis. Sorbonne Université. Paris, France.

Hugenschmidt, J., Kasa, C., Kato, H., 2013. GPR for the inspection of industrial railway tracks. Near Surface Geophysics 11, 485–492. doi:https://doi.org/10.3997/1873-0604.2013031.

Hwang, H.J., Park, H.C., 2014. Evaluation of condition of gravel ballast layer on high-speed railway using surface wave method based on harmonic wavelet analysis of waves. NDT & E International 68, 78–87. doi:10.1016/j.ndteint.2014.08.005.

Hévin, G., Abraham, O., Pedersen, H., Campillo, M., 1998. Characterization of surface cracks with Rayleigh waves: a numerical model. NDT & E International 31, 289–297. doi:https://doi.org/10.1016/S0963-8695(98)80013-3.

Karl, L., Fechner, T., Schevenels, M., François, S., Degrande, G., 2011. Geotechnical characterization of a river dyke by surface waves. Near Surface Geophysics 9, 515–527. doi:https://doi.org/10.3997/1873-0604.2011030.

Khakiev, Z., Shapovalov, V., Kruglikov, A., Yavna, V., 2014. GPR determination of physical parameters of railway structural layers. Journal of Applied Geophysics 106, 139–145. doi:https://doi.org/10.1016/j.jappgeo.2014.04.017.

Killingbeck, S., Livermore, P., Booth, A., West, L., 2018. Multimodal layered transdimensional inversion of seismic dispersion curves with depth constraints. Geochemistry, Geophysics, Geosystems 19, 4957–4971. doi:https://doi.org/10.1029/2018GC008000.

Kyrkou, K., Frost, M., Fleming, P., Sartain, N., Trinder, S., 2022. Seismic Surface Waves Methods for High-Speed Rail Earthworks Compliance: A Review of Measurement Practice, in: Proceedings of the 7 th World Congress on Civil, Structural, and Environmental Engineering (CSEE'22). doi:10.11159/icgre22.184.

Lai, C., Rix, G., 1998. Simultaneous inversion of Rayleigh phase velocity and attenuation for near-surface site characterization. Technical Report GIT-CEE/GEO-98-2.

Lai, C.G., Rix, G.J., Foti, S., Roma, V., 2002. Simultaneous measurement and inversion of surface wave dispersion and attenuation curves.

Soil Dynamics and Earthquake Engineering 22, 923–930. doi:https://doi.org/10.1016/S0267-7261(02)00116-1.

Lee, J., Santamarina, J., 2005. Bender elements: Performance and signal interpretation. Journal of Geotechnical and Geoenvironmental Engineering 131, 1063–1070. doi:https://doi.org/10.1061/(ASCE)1090-0241(2005)131:9(1063).

Lin, S., Ashlock, J.C., 2016. Improved seismic profiling by minimally invasive multimodal surface wave method with standard penetration test source (MMSW-SPT). Geophysical Journal International 208, 1308–1312. doi:https://doi.org/10.1093/gji/ggw471.

Maraschini, M., Ernst, F., Foti, S., Socco, L.V., 2010. A new misfit function for multimodal inversion of surface waves. Geophysics 75, G31–G43. doi:https://doi.org/10.1190/1.3436539.

Mari, J.L., Arens, G., Chapellier, D., Gaudiani, P., 2004. Géophysique de gisement et de génie civil. Technip.

Matthews, M.C., Hope, V.S., Clayton, C.R.I., 1996. The use of surface waves in the determination of ground stiffness profiles. Geotechnical Engineering 119, 84–95. doi:https://doi.org/10.1680/igeng.1996.28168.

Milsom, J., Eriksen, A., 2013. Field geophysics, 4^{th} edition. The geological field guides series, John Wiley & Sons.

Mokhtar, T.A., Herrmann, R.B., Russell, D.R., 1988. Seismic velocity and Q model for the shallow structure of the Arabian shield from short-period

Rayleigh waves. Geophysics 53, 1379–1387. doi:https://doi.org/10.1190/1.1442417.

Nazarian, S., Stokoe II, K., 1984. In situ shear wave velocity from spectral analysis of surface waves. Center for Transportation Research 3, 31–38.

Nebieridze, S., Leroux, P., 2012. Geotechnics, geophysics : a help to the earthwordks diagnosis example : the excavation of versigny, in: Journée Nationales de Géotechnique et de Géologie de l'Ingénieur, JNGG2012, France.

Neducza, B., 2007. Stacking of surface waves. Geophysics 72, V51–V58. doi:https://doi.org/10.1190/1.2431635.

O'Neill, A., 2003. Full-waveform Reflectivity for Modelling, Inversion and Appraisal of Seismic Surface Wave Dispersion in Shallow Site Investigations. Ph.D. thesis. The University of Western Australia, School of Earth and Geographical Sciences.

O'Neill, A., Dentith, M., List, R., 2003. Full-waveform P-SV reflectivity inversion of surface waves for shallow engineering applications. Exploration Geophysics 34, 158–173. doi:https://doi.org/10.1071/EG03158.

O'Neill, A., Matsuoka, T., 2005. Dominant Higher Surface-wave Modes and Possible Inversion Pitfalls. Journal of Environmental and Engineering Geophysics 10, 185–201. doi:https://doi.org/10.2113/JEEG10.2.185.

O'Donovan, J., O'Sullivan, C., Marketos, G., 2012. Two-dimensional discrete element modelling of bender element tests on an idealised granular material. Granular Matter 14, 733–747. doi:10.1007/s10035-012-0373-9.

Pasquet, S., 2014. Apport des méthodes sismiques à l'hydrogéophysique : importance du rapport Vp/Vs et contribution des ondes de surface. Theses. Université Pierre et Marie Curie. URL: https://tel.archives-ouvertes.fr/tel-01099300.

Pasquet, S., Bodet, L., 2017. SWIP: An integrated workflow for surface-wave dispersion inversion and profiling. Geophysics 82, WB47–WB61. doi:https://doi.org/10.1190/geo2016-0625.1.

Pasquet, S., Bodet, L., Longuevergne, L., Dhemaied, A., Camerlynck, C., Rejiba, F., Guérin, R., 2015. 2d characterization of near-surface Vp/Vs: surface-wave dispersion inversion versus refraction tomography. Near Surface Geophysics 13, 315–332. doi:10.3997/1873-0604.2015028.

Quiroga, L., Schnieder, E., 2013. Railway Systems. Springer Berlin Heidelberg, Berlin, Heidelberg. pp. 519–537. doi:https://doi.org/10.1007/978-3-642-25850-3_26.

Rejkjær, S., Finco, C., Schamper, C., Rejiba, F., Tabbagh, A., König, J., Dahlin, T., 2021. Determination of the resistivity distribution along underground pipes in urban contexts using galvanic and capacitive methods. Near Surface Geophysics 19, 27–41. doi:10.1002/nsg.12135.

Rhayma, N., Bressolette, P., Breul, P., Fogli, M., Saussine, G., 2013. Reliability analysis of maintenance operations for railway tracks. Reliability Engineering & System Safety 114, 12–25. doi:https://doi.org/10.1016/j.ress.2012.12.007.

Ryden, N., Ulriksen, P., Park, C.B., 2004. Surface waves in inversely dispersive media. Near Surface Geophysics 2, 187–197. doi:https://doi.org/10.3997/1873-0604.2004016.

Ryden, N., Ulriksen, P., Park, C.B., Miller, R.D., Xia, J., Ivanov, J., 2001. High frequency MASW for non-destructive testing of pavements–accelerometer approach, in: SAGEEP, EEGS. pp. 1–12. doi:https://doi.org/10.4133/1.2922937.

Sambridge, M., 1999a. Geophysical inversion with a neighbourhood algorithm - ii. appraising the ensemble. Geophysical journal international 138, 727–746. doi:https://doi.org/10.1046/j.1365-246x.1999.00900.x.

Sambridge, M., 1999b. Geophysical inversion with a neighbourhood algorithm-i. searching a parameter space. Geophysical journal international 138, 479–494. doi:https://doi.org/10.1046/j.1365-246X.1999.00876.x.

Santamarina, J., Rinaldi, V., Fratta, D., Klein, K., Wang, Y., Cho, G., Cascante, G., 2005. A Survey of Elastic and Electromagnetic Properties of Near-Surface Soils, in: Near-Surface Geophysics. Society of Exploration Geophysicists, pp. 71–88. doi:https://doi.org/10.1190/1.9781560801719.ch4.

Schmelzbach, C., Green, A., Horstmeyer, H., 2005. Ultra-shallow seismic reflection imaging in a region and characterized by high source-generated noise. Near Surface Geophysics 3, 33–46. doi:https://doi.org/10.3997/1873-0604.2004027.

Selig, E., Waters, J., 1994. Track Geotechnology and Substructure Management. Thomas Telford Publications, London.

Shirley, D.J., Hampton, L.D., 1978. Shear-wave measurements in laboratory sediments. The Journal of the Acoustical Society of America 63, 607–613. doi:https://doi.org/10.1121/1.381760.

Socco, L., Foti, S., Boiero, D., 2010. Surface-wave analysis for building near-surface velocity models—Established approaches and new perspectives. Geophysics 75, 75A83–75A102. doi:https://doi.org/10.1190/1.3479491.

Socco, L.V., Strobbia, C., 2004. Surface-wave method for near-surface characterization: a tutorial. Near Surface Geophysics 2, 165–185. doi:https://doi.org/10.3997/1873-0604.2004015.

Steinel, H., Hausmann, J., Werban, U., Dietrich, P., 2014. Reliability of MASW and profiling in near-surface applications. Near Surface Geophysics 12, 731–737. doi:https://doi.org/10.3997/1873-0604.2014029.

Sussmann Jr, T., Thompson II, H., Stark, T., Wilk, S., Ho, C., 2017. Use of seismic surface wave testing to assess track substructure condition. Construction and Building Materials 155, 1250–1255. doi:https://doi.org/10.1016/j.conbuildmat.2017.02.077.

Talfumiere, V., Nebieridze, S., 2008. Utilisation du bruit ambiant comme source sismique pour detecter des cavités - gare de l'est, in: Journées Nationales de Géotechnique et de Géologie de l'Ingénieur JNGG'08, pp.

369–376. URL: https://www.cfmr-roches.org/sites/default/files/jngg/JNGG%202008%20pp%20369-376%20Talfumiere.pdf.

Tarantola, A., 2005. Inverse Problem and Theory and Methods for Model and Parameter Estimation. Society for Industrial and Applied Mathematic.

Tarantola, A., Valette, B., 1982. Inverse problems= quest for information. Journal of Geophysics 50, 159–170. doi:https://n2t.net/ark:/88439/y048722.

Thomson, W.T., 1950. Transmission of elastic waves through a stratified solid medium. Journal of Applied Physics 21, 89–93. doi:https://doi.org/10.1063/1.1699629.

Trevin, J.M., 2008. Le Manuel de la Voie Ferrée. SNCF Réseau, La Plaine Saint-Denis, France.

Tzanakakis, K., 2013. The railway track and its long term behaviour: a handbook for a railway track of high quality. Springer.

Sample CRediT author statement

Audrey Burzawa: Conceptualization, methodology, software, investigation, Writing - Original Draft. **Ludovic Bodet**: Conceptualization, methodology, investigation, supervision, project administration, funding acquisition, Writing - Original Draft, Writing - Review & Editing. **Amine Dhemaied:** Conceptualization, methodology, investigation, supervision, project administration. **Marine Dangeard**: Conceptualization, methodology, investigation, supervision. **Sylvain Pasquet**: Investigation, Writing - Review & Editing. **Quentin Vitale**: Investigation, Writing - Review & Editing. **Joséphine Boisson-Gaboriau**: Writing - Review & Editing, supervision. **Yu-Jun Cui** : ressource, investigation, Writing - Review & Editing.

Declaration of interests

☒ The authors declare that they have no known competing financial interests or personal relationships that could have appeared to influence the work reported in this paper.

☐ The authors declare the following financial interests/personal relationships which may be considered as potential competing interests:

Highlights

Detecting mechanical property anomalies along railway earthworks by Bayesian appraisal of MASW data

A. Burzawa, L. Bodet, A. Dhemaied, M. Dangeard, S. Pasquet, Q. Vitale, J. Boisson-Gaboriau, Y. J. Cui

- Designing non-destructive tools allowing efficient diagnosis of railway earthworks
- Geotechnical and geophysical study of a test site along an High Speed Line
- Surface-wave seismic acquisition to delineate shear-wave velocity variations
- Correlation between shear-wave velocity decrease and abnormal maintenance efforts
- Shear moduli profile presented in probability to provide a decision support tool